# LTI MODELLING OF ACTIVE MAGNETIC BEARINGS BY MEANS OF SYSTEM IDENTIFICATION

**P.A. van Vuuren** *, **G. van Schoor** † **and W.C. Venter** ‡

* *School of Electrical, Electronic and Computer Engineering, North-West University, & Private Bag X6001, Potchefstroom, 2520, South-Africa. E-mail: Pieter.VanVuuren@nwu.ac.za*

† *E-mail: George.vanSchoor@nwu.ac.za*

‡ *E-mail: Willie.Venter@nwu.ac.za*

**Abstract:** A relatively unknown phenomenon in active magnetic bearings (AMBs) is that the frequency content of their rotor position signal can induce nonlinear behaviour in the bearings. The existence of such frequency-induced nonlinear behaviour is experimentally and theoretically confirmed. Frequency-induced nonlinearity is characterised by means of a novel graphical representation. The resultant graph is quite useful in the specification of suitable excitation signals when AMBs are to be modelled by means of system identification.

**Key words:** Active magnetic bearings, system identification, non-linear, LTI.

## 1. INTRODUCTION

Conventional bearings use lubricated contact surfaces to support a rotating axle. Despite centuries of development, friction remains a fact of life for conventional bearings. Friction causes loss of power and energy as well as limited component lifetime due to wear and tear. These problems can be avoided by employing magnets to support the rotating shaft by magnetic forces, thereby realising contactless and consequently frictionless rotation.

Magnetic bearings most frequently operate on the principle of an attracting magnetic force which suspends an object against gravity. Such magnetic bearings exhibit negative stiffness [1] and have to be actively controlled to ensure contactless levitation. Such bearings are called active magnetic bearings.

As can be seen from figure 1, the basic construction of a typical active magnetic bearing consists of a stationary stator enclosing the shaft/rotor. The stator contains several electromagnets that exert reluctance magnetic forces on the rotor, thereby suspending it against the force of gravity and preventing contact with the stator surface. Sensors mounted on the stator continually monitor the position of the rotor. These position signals are used by a controller to adjust the power amplifier that supplies each pole with the necessary current to suspend the rotor.

Accurate and reliable position sensors are critical components of a functioning AMB system. These sensors are however expensive. Self-sensing techniques attempt to estimate the position of the rotor from the electrical impedance of the stator electromagnet coils [2].

For self-sensing AMBs to be of practical worth, they have to be robust. Robustness analysis aims to quantify a control system's tolerance for uncertainty. Accurate robustness analysis of systems requires accurate models. The intricacies of some systems defy conventional analytical

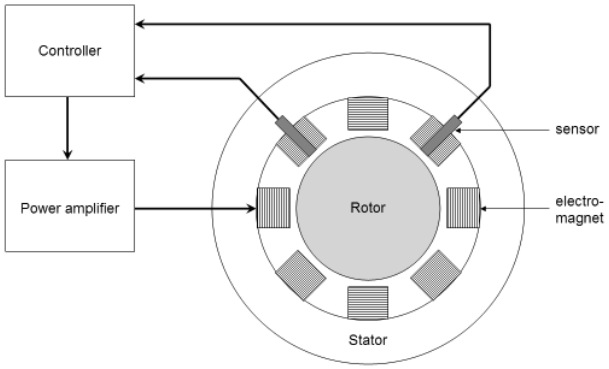


Figure 1: General structure of an AMB

modelling approaches and require a black-box system identification approach. This is the case in the robustness analysis of self-sensing AMBs. Self-sensing AMBs are quite sensitive to electromagnetic cross-coupling between the various electromagnets in the AMB stator [3], [4]. It is however quite difficult to obtain an accurate analytical model for electromagnetic cross-coupling in an AMB stator by means of first principles deductive modelling techniques. Fortunately, the required models can be easily obtained by means of system identification.

More details on the robustness analysis of a self-sensing AMB by means of $\mu$-analysis can be found in [5]. The focus of this contribution is on the influence of frequency induced nonlinear behaviour of AMBs on the choice of the excitation signal to be used for system identification. For this reason, this paper is only concerned with the application of system identification to AMBs equipped with explicit position sensors.

System identification has been applied in various forms and for various motives to AMBs. The most basic application of system identification concepts is the use of parameter estimation algorithms to obtain values for

parameters that can't be measured with conventional sensors. Examples of such parameters in AMBs are the damping and stiffness of the bearing that have been estimated by both discrete-time [6] and frequency domain system identification techniques [7].

Frequency domain system identification [8] has also been applied to obtain a single multivariable model for twin radial AMBs with a flexible shaft [9]. Their identified model encapsulated the power amplifiers, both AMBs, as well as the (non-rotating) rotor.

Discrete-time system identification [10] has been applied to a 1-DOF AMB with the purpose of modelling the nominal plant as well as its dynamic uncertainties [11]. Once again the "plant" contained everything except the controller, since the objective of the whole modelling process was to design an $H_\infty$ controller for the 1-DOF AMB. The same research team has since extended their work to twin radial bearings with a rotating flexible rotor [12].

The common denominator of the previous work performed on the application of system identification to AMBs is that the influence of frequency-induced nonlinear behaviour in the AMBs were ignored. This phenomenon is relatively unknown and entails that the rotor may suddenly reveal oscillatory behaviour or even delevitate if the rotor position is perturbed with a sufficiently high frequency disturbance signal. Evidence of this phenomenon in the literature is sparse. Simulation results by Hegazy and Amer show that changing the amplitude of excitation signals (external disturbance forces) may induce chaotic behaviour in the rotor [13]. These simulation results are supported by the experimental results of Jugo *et al.* [14]. They have shown that excessive vibrations (due to mechanical resonance at certain rotational speeds) result in loss in the low-frequency gain of the AMB. (In other words, the magnetic force falls away if the rotor is vibrated at certain frequencies.)

Accurate system identification however depends on persistent excitation [15]. An excitation signal that gives rise to maximally informative input and output data is known as a persistently exciting signal [10]. Persistent excitation is therefore determined by the frequency content of the excitation signal. It is consequently vital to ensure that nonlinear behaviour isn't induced in the AMB by the very signal with which it is interrogated. With this in mind, the next section explores the topic of frequency induced nonlinear behaviour in more detail. Amongst other things section 2. also introduces a useful graphical tool that classifies an AMB's behaviour into linear and nonlinear domains of operation as a function of the amplitude and frequency content of the rotor position signal. Section 3. summarizes the application of system identification to a 2-DOF AMB equipped with position sensors. Identified models are validated and evaluated in section 4., making the case for the inclusion of frequency induced nonlinear behaviour in the specification of the excitation signal for LTI system identification of AMBs.

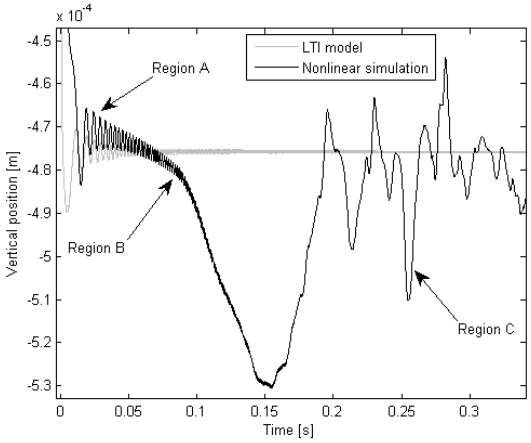


Figure 2: Simulated response of a nonlinear 1-DOF AMB to a frequency sweep

## 2. FREQUENCY INDUCED NONLINEAR BEHAVIOUR IN AMBS

### *2.1 Different regions of operation*

Figure 2 reveals the specific nonlinear behaviour induced by the frequency of the shaft position. This figure shows the simulated response of a 1-DOF sensed AMB for a reference position signal that consisted of a sine-wave frequency sweep at a constant amplitude. Also shown is the response of an identified LTI model of the 1-DOF AMB to exactly the same signal. For low frequencies, the nonlinear system behaves like a typical low-pass LTI system. As the frequency of the input signal is gradually increased, the nonlinear system departs from LTI behaviour in that its bias level starts to drift away from its initial value. A further increase in the input frequency however results in an abrupt change in the behaviour of the nonlinear system: it exhibits oscillatory motion with a frequency is much lower than that of the input signal. (In fact, this frequency is approximately the same as that of the dominant pole of the closed-loop LTI model for the system.) Not shown in figure 2 is the consequence of a further increase in the frequency of the input signal, namely delevitation of the AMB.

From the above discussion it seems as if frequency induced nonlinear behaviour in AMBs can be classified into four regions, namely:

- Region A: Pure LTI behaviour.
- Region B: Characterized by a drifting bias level, but otherwise similar to linear affine models.
- Region C: Oscillations occuring at a much lower frequency than that of the input signal.
- Region D: Delevitation.

Up to this point, the response of a 1-DOF AMB has been used to introduce frequency-induced nonlinear behaviour. 2-DOF AMBs also exhibit this kind of

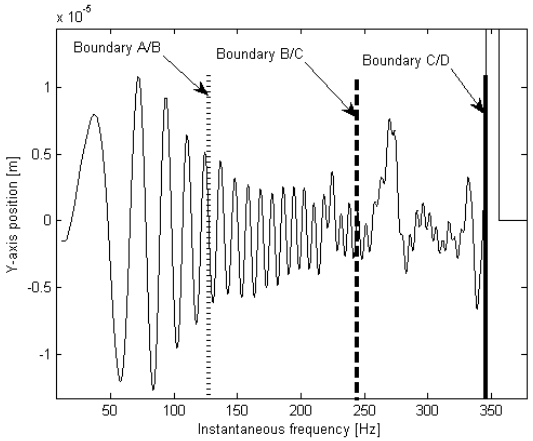


Figure 3: Simulated response of a nonlinear 2-DOF AMB to a frequency sweep

behaviour, as can be seen from figure 3. Only the y-axis component of the rotor position is shown (since the desired behaviour is more pronounced in the vertical dimension due to gravity). Although the AMB response in this figure is a function of time, it has been plotted against the instantaneous frequency of the input signal to accentuate the relationship between the AMB response and frequency. The (admittedly fuzzy) boundaries between the various regions of behaviour have been determined via an automatic algorithm described in [5].

### 2.2 *The cause of frequency induced nonlinearities*

The root cause of frequency-induced nonlinearities in AMB behaviour can best be explained by making use of the force equation (1) for a 1-DOF AMB. If only the top coil of an AMB is allowed to carry a current and electromagnetic cross-coupling is ignored, the force exerted by the resulting 1-DOF can be modelled by the following equation [1]:

$$f_m = \mu_0 \left( \frac{Ni}{l_c/\mu_r + 2x_g} \right)^2 A\cos(\theta), \tag{1}$$

with $l_c$ the length of the magnetic path (excluding the airgap);
$\mu_0$ the permeability of free space;
$\mu_r$ the relative permeability of the AMB stator;
$x_g$ the distance of the airgap between the stator and rotor;
$N$ the number of windings in the coil;
$i$ the current flowing in the coil;
$A$ the pole-face area; and
$\theta$ the angle between the vertical axis and the normal line to the pole face.

By collecting all constants in a single coefficient, $k$, the electromagnetic force exerted by a 1-DOF AMB can be modelled as follows (with all time-dependencies explicitly highlighted):

$$f_m(t) = k\frac{i^2(t)}{x_g^2(t)}. \tag{2}$$

Taking the derivative of (2) with respect to time allows us to investigate the effect that *changes* in the position of the rotor can have on the force exerted by the AMB on the rotor. Application of the quotient rule of differentiation results in the following:

$$\frac{df_m(t)}{dt} = \frac{2ki(t)\frac{di(t)}{dt}x_g^2(t) - 2ki^2(t)x_g(t)\frac{dx_g(t)}{dt}}{x_g^4(t)}. \tag{3}$$

Rearranging (3) with the aim of expressing the force of equation (2) in terms of the derivatives of position and current leads to:

$$f_m(t) = \frac{ki(t)\left(\frac{di(t)}{dt}\right)}{x_g(t)\left(\frac{dx_g(t)}{dt}\right)} - \frac{x_g(t)\left(\frac{df_m(t)}{dt}\right)}{2\left(\frac{dx_g(t)}{dt}\right)}. \tag{4}$$

From (4) it is clear that the force exerted by the AMB is inversely proportional to the derivative of the position of the rotor.* Sudden and large changes in the position of the rotor will therefore result in a commensurate loss in magnetic force applied to the rotor. Another conclusion stemming from (4) is that both the frequency and amplitude of the changes in the rotor position will lead to a reduction in the force. (The derivative of the position signal is after all not only determined by how quickly the input signal changes, but also by the amplitude of the change.)

### 2.3 *Frequency induced nonlinear behaviour in a physical AMB*

Before proceeding with the implications of frequency induced nonlinearities for system identification, experimental proof will be given for the existence of this phenomenon. The results presented in this section confirm the conclusions made by Jugo *et al.* in [14], but in a slightly different setting and with a different methodology. (Voltage controlled AMBs were used in [14], while our AMBs are current controlled. Furthermore, the results in [14] were obtained for a rotating shaft and required Floquet analysis, while our results are for a non-rotating rotor.)

*Experimental setup:* Our experimental setup consisted of a rigid rotor suspended horizontally between two eight-pole heteropolar radial AMBs [16]. The AMBs were designed for a peak load of 500 N and rms load of 200 N. The characteristic parameters of the AMBs are summarized in table 1 (some of which are elucidated in figure 4). Control of the system (and data capturing)

*A similar result can be obtained for a 1-DOF AMB equipped with two actuators operating in differential driving mode [1].

Table 1: Summary of the physical AMBs

| Parameter | Value |
|---|---|
| $K_P$ (position PD controller) | 20,000 |
| $K_D$ (position PD controller) | 38 |
| $K_P$ (power amplifier PI controller) | 1 |
| $K_I$ (power amplifier PI controller) | 0.01 |
| Relative magnetic permeability | 4,000 |
| Power amplifier switching frequency | 100 kHz |
| Supply voltage | 300 V |
| Bias current | 3 A |
| Resistance of coil wires | 0.2 Ω |
| Coil turns | 50 |
| Rotor mass | 12.5 kg |
| Airgap | 0.6 mm |
| Backup bearing inner radius | 250 $\mu m$ |
| Axial bearing length | 49.15 mm |
| Journal inner radius $(r_r)$ | 15.88 mm |
| Journal outer radius $(r_j)$ | 34.95 mm |
| Stator pole radius $(r_p)$ | 35.60 mm |
| Stator back-iron inner radius $(r_c)$ | 60.00 mm |
| Stator outer radius $(r_s)$ | 75.00 mm |
| Pole width $(r_w)$ | 13.89 mm |

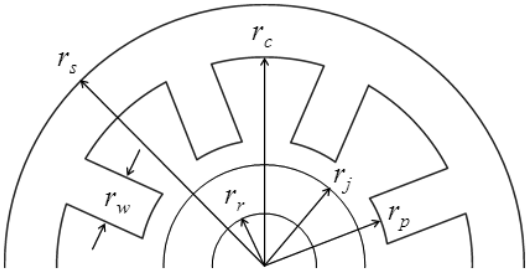


Figure 4: Physical dimensions of an AMB

is performed on a desktop PC by means of dSPACE real time hardware and Matlab/Simulink®. Each AMB is independently controlled by means of two identical decoupled PD controllers (each responsible for movement along a single dimension). All results given in this paper were measured on the left hand AMB (and not on the rotor's centre of mass).

*AMB response to a frequency sweep:* The response of the left hand AMB to a frequency sweep is shown in figure 5. The reference position signal consisted of a 100 μm (peak) amplitude sinewave applied to the *y*-axis input (and zero to the *x*-axis input). This signal's frequency was linearly changed from 10 Hz to 5 kHz over an interval of 20 seconds. (The use of a sinewave as well as a relatively long duration sweep minimizes transient effects in the AMB's response.)

The presence of some of the critical resonant frequencies of the rotor can be easily seen in the response of the AMB. Furthermore, a drifting DC level (region B behaviour) and a low frequency component which emerges at high

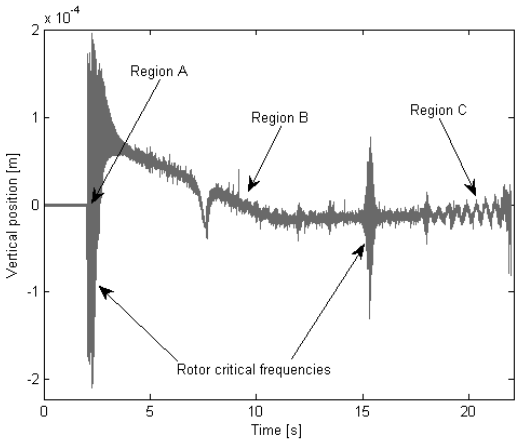


Figure 5: Measured AMB response to a 100 μm (peak) frequency sweep

frequency excitation (i.e. region C behaviour) are also visible. Clearly the response in figure 5 verifies the nonlinear behaviour predicted in the simulated responses of figures 2 and 3.

*Existence of subharmonic generation:* Mere inspection of a frequency sweep response however doesn't comprise proof of nonlinear behaviour. Nonlinear systems are characterised by subharmonic generation, where the output spectrum contains components at frequencies that are linear combinations of the input spectral components' frequencies. (In other words, if two frequencies $f_1$ and $f_2$ are present in the input signal, then the output signal contains components at the following frequencies $af_1 \pm bf_2$, where $a$ and $b$ are arbitrary integers [17].) Nonlinearity can therefore be diagnosed if subharmonic generation occurs.

Figure 6 shows the spectrum of the steady state response of the AMB when confronted with three sinusoidal inputs, namely two 10 μm (peak) sines at respectively 200 Hz and 300 Hz as well as a 40 μm (peak) sine at 3 kHz. The purpose of the latter signal is to induce nonlinear behaviour in the AMB, while the former two signals were chosen in order to obtain clearly visible results of subharmonic generation.

Figure 6 clearly shows the existence of a significant component at 100 Hz, which indicates subharmonic generation and consequently nonlinear behaviour. Also visible in this figure is a small very low-frequency component (despite the fact that the data was detrended prior to spectral analysis). Such low frequency components are indicative of emergent region C behaviour.

The influence of the amplitude and frequency of the high-frequency signal responsible for inducing nonlinear behaviour on the size of the low-frequency components is shown in figure 7. This figure was obtained by repeating the analysis performed to obtain figure 6 for various high frequency input signals. (I.e. the 200 Hz and 300 Hz input

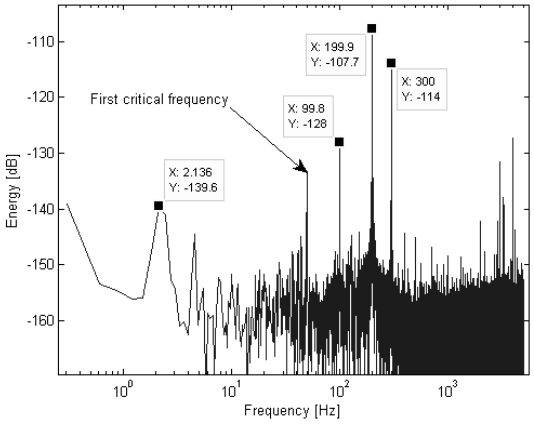


Figure 6: Y-axis spectrum in response to three input signals

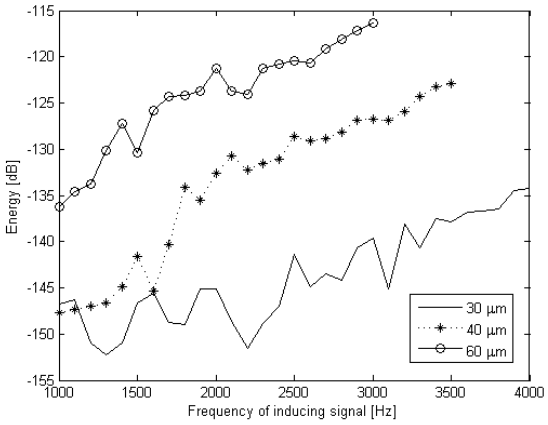


Figure 7: Size of the 2.2 Hz component as a function of the amplitude and frequency of a high frequency inducing signal.

signals were kept unaltered, but the third input signal was modified in both its amplitude and frequency.) Clearly the size of the low-frequency oscillation characteristic of region C behaviour is strongly influenced by both the amplitude and frequency of the inducing signal.

### *2.4 The frequency-amplitude graph*

Whether an AMB behaves linearly or nonlinearly depends on both the amplitude and frequency of the rotor position signal. The behaviour of an AMB for various combinations of frequencies and amplitudes of the input signal can be summarized in a single graph. Figure 8 presents the basic idea of a possible graphical AMB characterization tool. This graph is based on the response of an AMB to numerous frequency sweeps (of various combinations of the amplitude and maximum frequency reached during the sweep). This graphical tool gives an immediate indication of the expected fidelity of an LTI model for the AMB for different input signals.

The conceptual graph in figure 8 can only be realized in practice if the boundaries between regions A, B, C and D

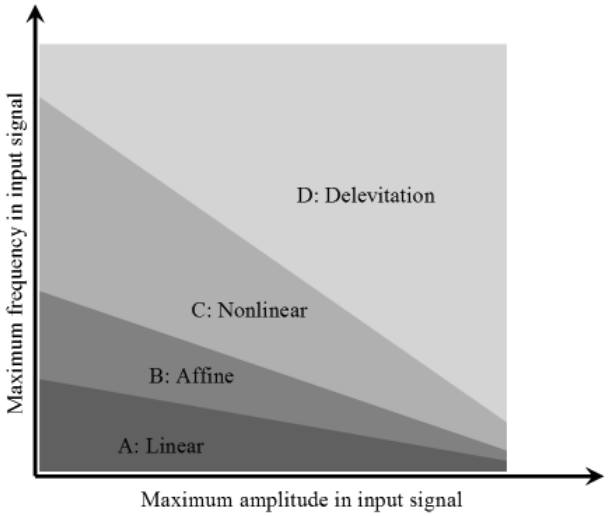


Figure 8: Conceptual frequency-amplitude graph of an AMB

can be automatically detected. Although the progression from one region to the next occurs gradually, it is possible to detect the boundaries between them on the basis of the observed system response. This can be done by clearly defining the onset of region B, C and D behaviour.

Delevitation (region D) is easy to detect since it occurs when the radial position of the point mass exceeds the inner diameter of the retainer bearing (in this case 250 µm). Similarly, region B behaviour can be defined as the first occurence of a trend (in any direction) in the bias level of the AMB response. This leaves region C behaviour which can be defined as oscillations with a period that is significantly longer than the period of the input signal. One possible automatic algorithm that performs the above mentioned classification is discussed in detail in [5].

As an example, figure 9 shows the frequency-amplitude graph obtained for a representative nonlinear simulation model of a 2-DOF AMB. This graph shows that a surprisingly large subset of input signals will induce nonlinear behaviour in an AMB. (Most of these signals are however outside the typical operating range of AMB applications.)

The nonlinear simulation model with which figure 9 was generated consists of a controller, four power amplifiers, a magnetic circuit model, point mass and ideal position sensors. The accuracy of this simulation model has been established in a previous study by comparison with experimental results [18]. Similar to the physical AMB system, the controller consists of two identical decoupled PD controllers, each responsible for one axis of movement. Each of the four stator electromagnets is powered by its own two-state switched mode power amplifier. The duty cycle of each of these amplifiers is constrained to remain within the interval of 25 % to 75 % and is controlled with a PI controller.

The remainder of the sensed-AMB simulation model is

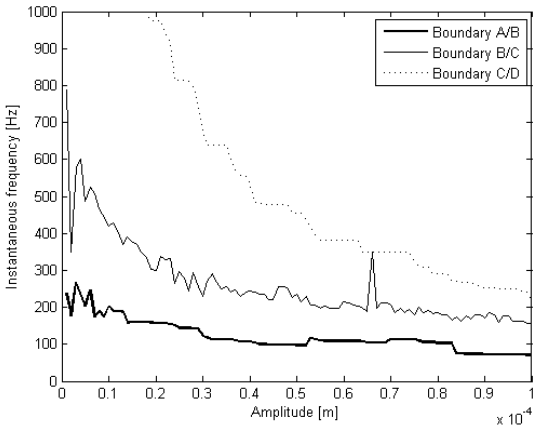


Figure 9: Frequency-amplitude graph for a simulated AMB

concerned with the AMB plant, which is dominated by the electromagnetic calculations required to model the force exerted on the point mass. A reluctance network model is used to model the flux distribution in the AMB magnetic circuit [19]. The response of the reluctance network model is enriched with two additional models: one responsible for predicting eddy currents and the other for modelling magnetic hysteresis and saturation. The final electromagnetic force exerted by the AMB on the point mass is proportional to the square of the magnetic flux density [1], [18]. Finally, the physical movement of the point mass is determined by means of the well-known Newton laws.

Armed with a frequency-amplitude graph such as figure 9, it is now possible to perform system identification to obtain accurate models for various parts of an AMB's operating domain (whether linear or nonlinear).

## 3. SYSTEM IDENTIFICATION APPLIED TO AMBS

### *3.1 Injection points and measuring points*

Applying system identification to AMBs is a challenging exercise due to the inherent instability of magnetic bearings. Since open-loop operation of an AMB is impossible, system identification must be performed while the AMB is in closed-loop operation. Various approaches exist to perform closed-loop system identification [10]. Of these, direct identification is the simplest to apply, yet is still able to model unstable plants. Direct identification entails that the control system be operated in closed-loop while the system is subjected to a small perturbation applied anywhere in the loop. The desired subsystem in the loop can then be modelled by merely extracting data from its specific inputs and outputs [10].

Empirical models are however only as good as the data from which they are derived. In system identification, the nature and quality of the model that is eventually identified is to a large extent determined by the excitation signal used [20]. The attribute required of excitation signals is

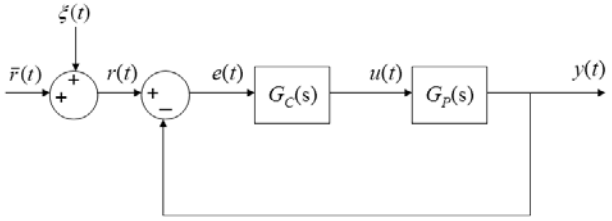


Figure 10: SISO closed-loop control system

*persistent excitation*. The main feature of a persistently exciting excitation signal is that its power spectrum must be as flat as possible (within a specified frequency band) [15].

Unfortunately the primary advantage of negative feedback, namely that feedback reduces the closed-loop system's sensitivity for disturbances to the plant [20], complicates matters for closed-loop system identification. The nett effect of feedback is that the reduced sensitivity of the system results in less informative data for parameter estimation [10]. Even though an excitation signal may conform to the standards of persistent excitation, the specific point in the closed-loop control system at which it is applied may influence the extent to which the excitation signal is distorted before it arrives at the AMB input.

As an example, consider the simple SISO (single-input, single-output) control system in figure 10, where a controller, $G_C(s)$ is placed in series with a plant, $G_P(s)$. If the excitation signal $(\xi(t))$ is added to the nominal system reference signal $(\bar{r}(t))$, the resultant input to the plant is a filtered version of the original excitation signal, as is evident in (5),

$$\begin{aligned} U(s) &= G_C(s)E(s) \\ &= \frac{G_C(s)R(s)}{1+G_C(s)G_P(s)} \\ &= G_C(s)\bar{R}(s)S(s)+G_C(s)S(s)\Xi(s), \end{aligned} \quad (5)$$

where $S(s)$ represents the SISO sensitivity function.

### *3.2 Sampling frequency and model inputs and outputs*

In a typical AMB, the controller is known exactly. (In this case it consists of a pair of identical decentralized PID controllers, each responsible for one axis of movement within the airgap.) The only component that has to be modelled by means of system identification is the AMB plant which consists of the power amplifiers, AMB stator and rotor. (Separate models can be identified for the various components of the AMB plant if the aim is to assess the impact of the components on the total system stability robustness [5].) In this work, the AMB plant accepts two inputs from the controller. The first of these two inputs serves as a current reference signal for the power amplifiers of the top and bottom coils in the AMB stator, while the other input supplies a current reference to the remaining two power amplifiers of the left and right

stator coils. The two outputs of the identified AMB plant model represent the *x*-axis and *y*-axis position of the rotor within the airgap.

At present, it is easier to model multivariable systems by means of discrete-time system identification than with continuous-time techniques.** This work therefore makes use of discrete-time system identification to model a 2-DOF AMB. Prior to the application of a parameter estimation algorithm, it is necessary to choose the sampling frequency of the eventual models.

System identification works best if the sampling frequency is commensurate with the dominant time constants of the plant [10]. The lower bound on the sampling frequency is dictated by the Nyquist frequency of the phenomenon that has to be modelled. The natural frequency of the AMB under consideration in this work is approximately 63 Hz [16]. If the sampling frequency is chosen too high, numerical problems may arise during parameter estimation. Furthermore, the resultant model may contain too many high frequency dynamics and loose its focus on the important low frequency characteristics of the system. High sampling frequencies can also lead to nonminimum phase models [10]. In this work, the sampling frequency of the model is chosen the same as the sampling frequency of the implemented digital control system, namely 10 kHz.

### *3.3 Parameterized model structures*

The next step is to choose a suitable parameterized model structure. This choice has far reaching effects since an incorrect model structure contributes to the bias error of the model [10]. The two criteria that influence this choice are firstly the fact that the AMB plant is multivariable. Secondly, the model structure must have the capability to model unstable plants. (The AMB plant is after all inherently unstable and should therefore also be modelled as such.)

Various model structures are available with which MIMO (multi-input, multi-output) systems can be modelled. At present, the Matlab® system identification toolbox is limited to multivariable ARX (autoregressive with external inputs) and state-space model structures. Of these two, the state-space model structure is inherently an easier and more elegant framework to extend to multivariable problems.

The inherent instability of AMBs should however also be taken into consideration. ARX models are suitable for direct closed-loop identification of unstable systems [22]. The primary drawback of ARX models is that they may exhibit a slight high-frequency bias if the sampling frequency is too large [10], which manifests itself in the form of very large transient responses.

It is however possible to obtain unstable state-space models via system identification provided that the correct weighting scheme of the residuals is used during parameter estimation. If the weighting function is calculated as the product of the spectrum of the input signal and the inverse of the estimated noise model, then unstable plant models may ensue, provided that the correct model order is chosen. This weighting scheme is known as a "prediction focus", because it basically entails minimizing the one-step ahead prediction error of the model [23]. The resultant models admittedly have a high-frequency bias, yet don't exhibit the same large transients as ARX models do.

The model structure of choice is therefore state-space models, since it is possible to estimate both stable and unstable models for multivariable systems with them.

### *3.4 Parameter estimation algorithm*

A related issue to the model structure is the specific parameter estimation algorithm with which its parameters can be obtained. Broadly speaking, parameter estimation algorithms for state-space models can be dichotomized into two slightly overlapping families of algorithms, namely prediction error methods (PEM) and subspace methods [24].

PEM algorithms lay claim to optimal solutions of the parameter vector (in terms of the cost function that was used). Unfortunately, this advantage comes at the cost of increased computation time. (PEM algorithms converge iteratively to the "optimal" solution.) In contrast, subspace methods are non-iterative and therefore extremely fast, with only a slight bias error in their final estimates of the parameter vector [24]. In fact, Favoreel *et al.* have found that subspace methods performed quite satisfactorily on a range of industrial identification problems compared to PEM [24]. In practical applications, subspace methods regularly provide the initial estimate from which PEM algorithms proceed to the final solution [24], [23]. This approach is also followed in this study.

### *3.5 Excitation signal*

The utility of the frequency-amplitude graph becomes evident when it is used as a tool to evaluate potential excitation signals. Take for example the frequency-amplitude graph of figure 9. The effect that a particular excitation signal will have on the AMB's behaviour can be predicted by superimposing the spectral content of the excitation signal onto the vertical axis of the frequency-amplitude graph. In this way it is possible to see in advance whether a particular signal will induce region B or C behaviour in the AMB. This has been done for the case of white noise in figure 11. The superimposed spectrum clearly shows the characteristic flat spectrum of white noise. Furthermore, it is also evident that this excitation signal contains significant components in region B and C (at the specified amplitude). Consequently, it should come as no surprise that this excitation signal does induce nonlinear behaviour in the AMB.

What is required is an excitation signal whose spectral

**Current Matlab® toolboxes for continuous-time system identification are limited to SISO systems [21]

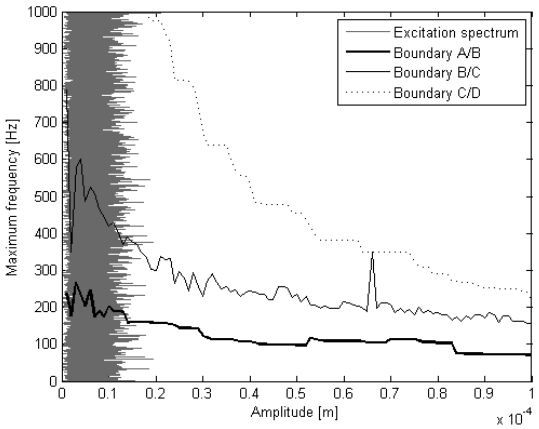


Figure 11: Evaluation of potential excitation signals: white noise

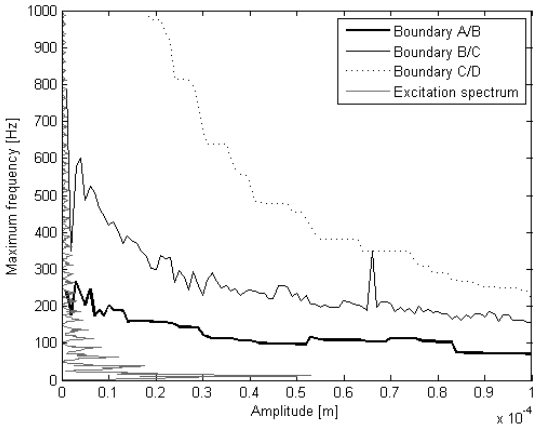


Figure 12: Evaluation of potential excitation signals: rectangular pulses

content can be constrained to be within a narrow band. Examples of such signals are random phase multi-sine signals and rectangular waves. Rectangular waves are ideal excitation signals for LTI system identification, since their spectrum falls away rapidly for increasing frequencies. If the amplitude of the rectangular wave is specified prudently, the AMB will remain within its LTI operating domain (see figure 12).

## 4. RESULTS

The results presented in this section underscore the usefulness of the frequency-amplitude graph introduced in section 2.4 for characterising and modelling AMBs. It is shown that accurate LTI models can be identified for the AMB provided that the excitation signal is confined to region A behaviour.

To obtain an accurate LTI model of the AMB plant, the excitation signal should be persistently exciting, yet short in duration and conform to the requirements of linear operation dictated by the AMBs frequency-amplitude graph. One such signal consists of square waves applied

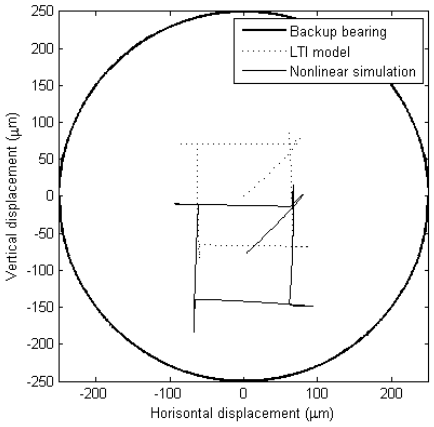


Figure 13: Orbital plot of the AMB response to the excitation signal

to the $x$- and $y$-axes independently thereby exposing the dynamics of the AMB in both directions separately while including enough information of cross-coupling between the horizontal and vertical dimensions. This signal's amplitude was limited to 50 μm in order to prevent the occurence of position-induced nonlinear behaviour in the AMB.

Through a process of trial and error a tenth order state-space model was fitted for the AMB plant. The closed-loop simulation performance of this model is compared to the response of the original nonlinear simulation for the AMB in figures 13 and 14. Figure 13 is an orbital plot of the responses of the nonlinear simulation model of the AMB as well as the LTI closed-loop model for it. This figure clearly shows that the LTI model can replicate the general pattern of the original response, but can't correctly model the DC offset in the vertical dimension. The latter shortcoming is to be expected since the LTI model for the plant was fitted on detrended data (as is standard practice in the system identification literature [10]). (This bias error can be easily corrected by merely adding the mean values of the actual AMB responses to the plant state-space model, as can be seen in figure 15.) The dynamic response of the AMB is however satisfactorily modelled by the LTI model as can be seen in figure 14 (which shows the responses of figure 13 as a function of time).

The LTI model of figures 13 and 14 is however only valid while the AMB is confined to linear behaviour. The inability of an LTI model to accurately model an AMB that exhibits frequency-induced nonlinear behaviour is visible in figure 15. This figure shows the response of the AMB when it is exposed to a 50 μm amplitude frequency sweep stretching from 11 Hz to 400 Hz which is applied concurrently to both the $x$- and $y$-axes. At higher frequencies the AMB's behaviour clearly becomes increasingly nonlinear.

The closed-loop response of the same LTI model of figures

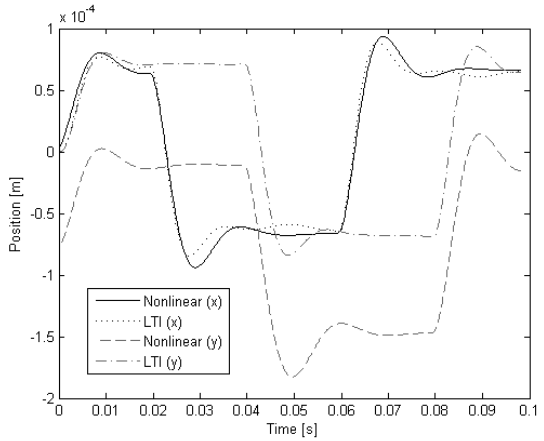


Figure 14: Response of the AMB models to the excitation signal

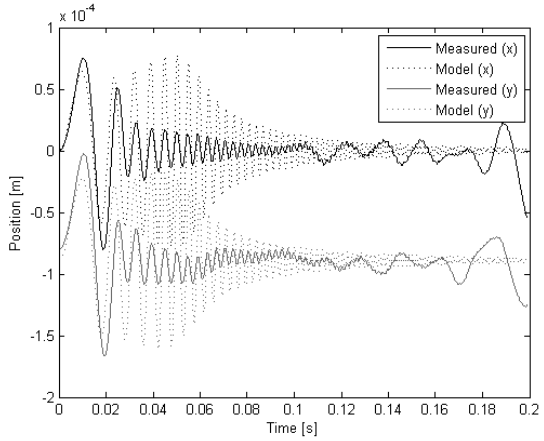


Figure 15: Response of the AMB models to a sine sweep

13 and 14 to the frequency sweep shows that this model is only representative of the AMB behaviour at very low frequencies (which is to be expected since the model was obtained on region A data). Region C behaviour can't be modelled by this LTI model. The inability of LTI models to replicate region B and C behaviour is underscored by the fact that not a single stable closed-loop LTI model could be obtained on excitation data that contained region B and C behaviour. (An example of such an excitation signal is a 50 μm amplitude random phase multi-sine signal applied to both axes concurrently. This signal's spectrum is almost uniform in a bandwidth from 11 Hz to 400 Hz and falls away rapidly outside this band.)

## 5. CONCLUSION

We have seen that nonlinear behaviour can be induced in AMBs by the frequency content and amplitude of the rotor position signal (and therefore also by the reference position signal). Consequently, the characteristics of the excitation signal used for system identification has a definite impact on the nature of the AMB (whether it can be viewed as a linear or nonlinear system). This means that the amplitude and spectral characteristics of the excitation signal has a large influence on the quality of the resultant LTI model obtained by means of system identification. Alternatively put, LTI system identification only gives accurate results if the excitation signal is chosen such that the AMB is constrained to LTI behaviour. Suitable excitation signals can be synthesized by means of the frequency-amplitude graph of figure 9, since this graph is a convenient summary of the degree of nonlinearity present in the AMB behaviour.

The frequency-amplitude graph can be of potential benefit in the design of controllers that must be able to stably suspend high-speed rotors. Another application of this graph is also the robustness analysis of self-sensing AMBs by means of $\mu$-analysis (which requires system identification and detailed uncertainty modelling).

## REFERENCES

[1] G. Schweitzer, H. Bleuler, and A. Traxler, *Active Magnetic Bearings: Basics, Properties and Applications of Active Magnetic Bearings*. Zürich: Authors Reprint, 2003.

[2] E. Maslen, "Magnetic bearing sensors," in *Short course on magnetic bearings*, 1997.

[3] N. Skricka and R. Markert, "Influence of cross-axis sensitivity and coordinate coupling on self-sensing," in *Proceedings of 6th International Symposium on Magnetic Suspension Technology*, Turin, Italy, October 2001, pp. 179–184.

[4] A. Niemann, "Self-sensing algorithms for active magnetic bearings," Ph.D. dissertation, North-West University, 2008.

[5] P. Van Vuuren, "Robustness estimation of self-sensing active magnetic bearings via system identification," Ph.D. dissertation, North-West University, 2010.

[6] S.-J. Kim and C.-W. Lee, "On-line identification of current and position stiffnesses by lms algorithm in active magnetic bearing system equipped with force transducers,," *Mechanical Systems and Signal Processing*, vol. 13, no. 5, pp. 681–690, 1999.

[7] T. Lim and S. Cheng, "Parameter estimation and statistical analysis on frequency-dependent active control forces," *Mechanical Systems and Signal Processing*, vol. 21, pp. 2112–2124, 2007.

[8] J. Schoukens and R. Pintelon, *Identification of linear systems: a practical guideline to accurate modeling*. Oxford: Pergamon press, 1991.

[9] C. Gähler, M. Mohler, and R. Herzog, "Multivariable identification of active magnetic bearing systems," *JSME international journal. Series C, Mechanical systems, machine elements and manufacturing*, vol. 40, no. 4, pp. 584–592, 1997.

[10] L. Ljung, *System identification: theory for the user*, 2nd ed. Upper Saddle River, NJ: Prentice Hall, 1999.

[11] N. Gibson, H. Choi, and G. Buckner, "$h_\infty$ control of active magnetic bearings using artificial neural network identification of uncertainty," in *2003 IEEE International Conference on Systems, Man and Cybernetics*, vol. 2, Washington D.C., 2003, pp. 1449–1456.

[12] H. Choi, G. Buckner, and N. Gibson, "Neural robust control of a high-speed flexible rotor supported on active magnetic bearings," in *Proceedings of the 2006 American Control Conference*, Minneapolis, Minnesota, June 2006, pp. 3679–3684.

[13] U. Hegazy and Y. Amer, "A time-varying stiffness rotor-active magnetic bearings system under parametric excitation," *Proc. IMechE Part C: J. Mechanical Engineering Science*, vol. 222, pp. 447–458, 2008.

[14] J. Jugo, I. Lizarraga, and I. Arredondo, "Nonlinear modelling and analysis of active magnetic bearing systems in the harmonic domain: a case study," *IET Control Theory Applications*, vol. 2, no. 1, pp. 61–71, 2008.

[15] Y. Cho, S. Srinavasan, J.-H. Oh, and H. Kim, "Modelling and system identification of active magnetic bearing systems," *Mathematical and Computer Modelling of Dynamical Systems*, vol. 13, no. 2, pp. 125–142, April 2007.

[16] E. Ranft, "The development of a flexible rotor active magnetic bearing system," Master's thesis, North-West University (Potchefstroom Campus), 2005.

[17] S. Shinners, *Modern control system theory and design*. New York: John Wiley & Sons, 1992.

[18] E. Ranft, "An improved model for self-sensing heteropolar active magnetic bearings," Ph.D. dissertation, North-West University (Potchefstroom campus), 2007.

[19] D. Meeker, E. Maslen, and M. Noh, "An augmented circuit model for magnetic bearings including eddy currents, fringing, and leakage," *IEEE Transactions on Magnetics*, vol. 32, no. 4, pp. 3219–3227, July 1996.

[20] H. Hjalmarsson, "From experiment design to closed-loop control," *Automatica*, vol. 41, pp. 393–438, 2005.

[21] I. Kollar, *Frequency Domain System Identification Toolbox: For Use with Matlab*, Vrije Universiteit Brussel, 2001. [Online]. Available: http://elecwww.vub.ac.be/fdident/

[22] P. Van Den Hof, "Closed-loop issues in system identification," *Annual reviews in control*, vol. 22, pp. 173–186, 1998.

[23] *Matlab*, R2008a ed., The MathWorks.

[24] W. Favoreel, B. De Moor, and P. Van Overschee, "Subspace state space system identification for industrial processes," *Journal of Process Control*, vol. 10, pp. 149–155, 2000.